# Nonlinear Kinematics and Force Analyses of A Cable-Driven Soft Finger

Po Ting Lin, Kai-An Yang, Cheng-Hsiu Chuang, and Yu-Ta Yao

***Abstract*—Soft robotics have been one of the most popular research topics in the fields of robotics and automation due to their advantages of higher flexibility and safer operations. Researches of soft robots are more complicated than the ones of traditional rigid robots because it's harder to control the movements of soft robots, or estimate their force reactions. Finite Element Analysis (FEA) could be used to analyze how the soft robot deforms but nonlinear FEA is required for large-deformation analysis. Another method to analyze the soft robot movement is to perform experiments and parametrically model the motions. A cable-driven soft finger was designed and utilized for the nonlinear kinematics analysis. The soft finger was made of Polydimethylsiloxane (PDMS) with 3D-printed bone structures. Parametric Denavit-Hartenberg (DH) Functions were used to mathematically describe the motions of soft robots under various levels of actuations. Furthermore, the gripping force of the soft finger was estimated based on a simple force model. The proposed nonlinear kinematics and force analysis could be applied to various kinds of soft robotics mechanisms.**

***Index Terms*—Soft Gripper, Polydimethylsiloxane (PDMS), 3D Printing, Kinematics, Denavit-Hartenberg (DH) Parameters.**

## I. Introduction

RECENTLY, researchers have been developing novel technologies in the field of soft robots because of the advantages of flexibility and safety. Soft robots have closer motions to human or other live creatures and have less chances of damaging the surrounding objects or human. Soft robotics have been widely applied to various applications such as medical devices [1], soft wearable robots [2], rehabilitation devices [3], grippers [4, 5], etc. In 2016, Wehner, et al. [6] presented a soft robot that is completely soft and could be controlled remotely. Their research results showed promising potentials of soft robots in manipulations, locomotion, and many other applications [7, 8]. Researchers have developed many novel manufacturing methodologies [9-11] to build soft robots as other researchers focused on control [12-15] of soft robots.

Unlike rigid robots, soft robots are harder for modeling. Lu, et al. [16] studied how large-deflection beams deform under various levels of pulling actuations. They also studied how the deformations changed with contacts of obstacles. Although large-deformation Finite Element Analysis (FEA) could be used to generate the digital twins of the soft actuators, it's very difficult to have reasonably accurate FEA models due to incorrect material properties, nonlinear material behaviors, inappropriate contact conditions, etc. Shahabi, et al. [17] used cameras to capture the soft finger actuations. Geometrical features were tracked and their 3D positions were measured. These 3D coordinates were used to compute how much the soft finger bends and twists during the actuations.

Denavit-Hartenberg (DH) parameters [18] have been used for the forward and backward kinematics of rigid robots with finite amount of rigid bodies and connection joints. However, it's hard to define the links and joints in soft robots, or one could say soft robots have infinite number of links and joints. Lin, et al. [19] have presented how to use parametrically modeled DH functions for soft robot kinematics. In this paper, the design and manufacturing of a cable-driven soft finger were presented. Parametric DH functions were used to investigate the kinematics of the soft finger based on various kinds of joint definitions. This paper also presented a methodology to estimate the gripping force of the soft finger. Visual inspections were used to measure and model the soft finger deformations under various levels of actuation forces. A simple force model was defined to estimate the gripping force at the tip of the soft finger.

## II. Design and Manufacturing of A Cable-Driven Soft Finger

In this paper, Polydimethylsiloxane (PDMS) was used to make a soft finger design. Cable was used to actuate the soft finger. Fig. 1 shows the parts that were used to make the soft finger. Two lower molds, that were made by 3D printing, forming the shape of the soft finger. Multiple embedding parts, that were also made by 3D printing, would be inserted into the soft finger to serve as bone structures inside the soft finger and provide some rigidity to the finger structure. Screws and nuts were used to tighten the lower molds and prevent the uncured PDMS leaking from the molds. A tube with a rod was inserted through the embedding parts to create a through hole in the soft finger. The through hole would be used for the installation of the driving cable.

This paper was first submitted in December 5, 2020. This work was supported by Ministry of Science and Technology (grant numbers MOST 106-2221-E-033-025, MOST 107-2221-E-011-088 and MOST 108-2221-E-011-129-MY3), and Center for Cyber-Physical System Innovation, which is a Featured Areas Research Center in Higher Education Sprout Project of Ministry of Education (MOE), Taiwan (since 2018).

Po Ting Lin is the corresponding author of this paper. Dr. Lin is an Associate Professor in the Department of Mechanical Engineering at National Taiwan University of Science and Technology (NTUST), Taipei 10609, Taiwan (e-mail: potinglin@mail.ntust.edu.tw).

Kai-An Yang was a MS student in the Department of Mechanical Engineering at NTUST, Taipei 10609, Taiwan and graduated in July 2019 (e-mail: sds121556622@gmail.com).

Cheng-Hsiu Chuang was a MS student in the Department of Mechanical Engineering at NTUST, Taipei 10609, Taiwan and graduated in July 2020 (e-mail: scsh10211paul@gmail.com).

Yu-Ta Yao was a MS student in the Department of Mechanical Engineering at NTUST, Taipei 10609, Taiwan and graduated in July 2020 (e-mail: pommyyao@gmail.com).

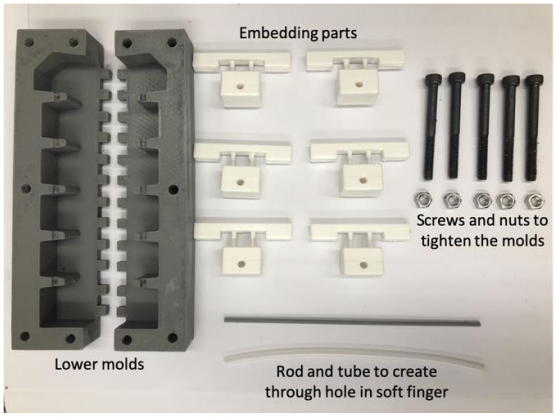


Fig. 1. Parts for making the soft finger, including two pieces of lower molds, six embedding parts which would be inserted into the uncured PDMS, screws and nuts for tightening the molds during the process of curing PDMS, and a rod and a rube for creating a through hole in the soft finger for installation of the cable.

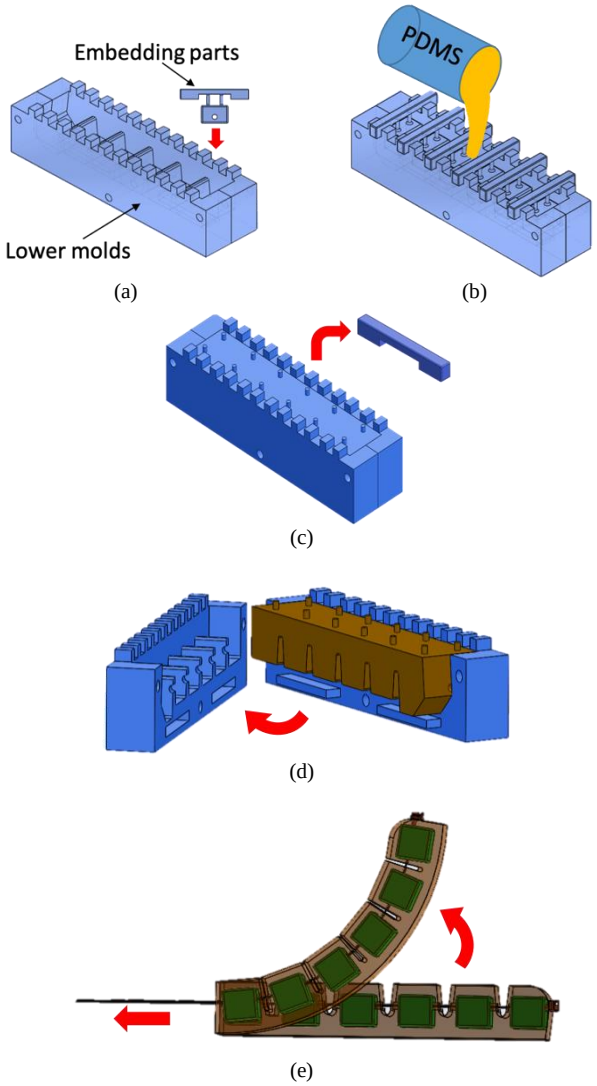


Fig. 2. Procedure of making the cable-driven soft finger [19]: (a) assemble the lower molds and insert the embedding parts into the mold; (b) pour the 10:1 mixed PDMS into the mold; (c) cure the PDMS and remove the supporting materials; (d) open the lower molds to release the soft finger; (e) insert the cable into the soft finger and pull to actuate the finger.

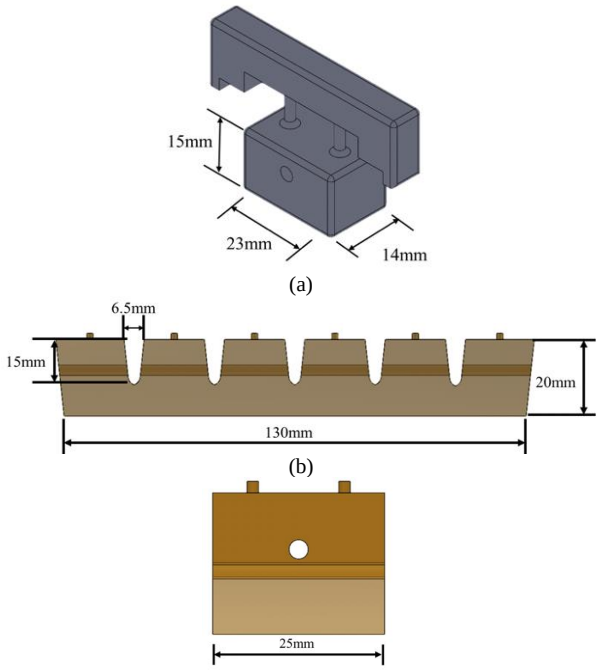


Fig. 3. Dimensions of the soft finger parts: (a) angular view of the embedding part shown in Fig. 2 (a); (b) side view of the released soft finger shown in Fig. 2 (d); (c) front view of the finger where the center hole is for the insertion of the cable.

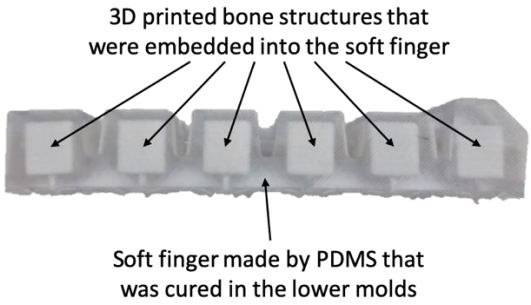


Fig. 4. Final production of a soft finger with embedded bone structures.

Fig. 2 shows the procedure of making the soft finger. As shown in Fig. 2 (a), the lower molds were first assembled together and tightened by the screws and nuts. The rod and tube, shown in Fig. 1, were inserted into the embedding parts as the embedding parts were inserted into the mold. The next step was to pour the 10:1 mixed PDMS into the mold, as shown in Fig. 2 (b), and degassed in a vacuum chamber. After the PDMS was cured, the supporting materials of the embedding parts were cut away, as shown in Fig. 2 (c). The lower molds were then disassembled to release the soft finger, shown in Fig. 2 (d). Finally, the cable was inserted into the soft finger. Pulling the cable would actuate the soft finger, as shown in Fig. 2 (e). When the pulling force was released, the soft finger would recover back to its original shape due to its own resilience.

The dimensions of the soft finger parts are shown in Fig. 3. Fig. 3 (a) shows the angular view of the embedding part, which was mentioned in both Fig. 1 and Fig. 2 (a). The rectangular box at the bottom half of the embedding part was to be inserted into

the lower molds and would serve as the bond structure inside the soft finger. The dimension of the rectangular box is 23 ´ 14 ´ 15 mm$^3$. Fig. 3 (b) and (c) show the dimension of the released soft finger. The grooves on the top side of the soft finger have an opening width of 6.5 mm, as shown in Fig. 3 (b), where each groove allows around 13~18 ° of bending. Fig. 4 shows how the final production of the soft finger with embedded bone structures looks like.

## III. Kinematics Analysis of the Soft Finger

Suppose a $i^{th}$ link is connected to a $(i-1)^{th}$ link at the $i^{th}$ joint, the angle between these two links is called the axis angle $q_i$. The offset between these two links along the $i^{th}$ joint is denoted as $d_i$. The length of the $i^{th}$ link is $a_i$. The twisted angle between the $i^{th}$ and the $(i+1)^{th}$ joints is denoted as $a_i$. Based on these DH parameters, the transformation of the $i^{th}$ link is given by:

$$ {}^{i-1}\mathbf{T}_i = \begin{bmatrix} \cos\theta_i & -\sin\theta_i & 0 & 0 \\ \sin\theta_i & \cos\theta_i & 0 & 0 \\ 0 & 0 & 1 & d_i \\ 0 & 0 & 0 & 1 \end{bmatrix} \cdot \begin{bmatrix} 1 & 0 & 0 & a_i \\ 0 & \cos\alpha_i & -\sin\alpha_i & 0 \\ 0 & \sin\alpha_i & \cos\alpha_i & 0 \\ 0 & 0 & 0 & 1 \end{bmatrix} \quad (1) $$

The coordinate of the end effector of a linkage robot with $N$ links is then given by:

$$ {}^0\mathbf{P} = {}^0\mathbf{T}_1\,{}^1\mathbf{T}_2 \cdots {}^{i-1}\mathbf{T}_i \cdots {}^{N-1}\mathbf{T}_N\,{}^N\mathbf{P} \quad (2) $$

where ${}^0\mathbf{P}$ and ${}^N\mathbf{P}$ are the coordinates of the end effector relative to the base frame and the end frame, respectively.

Suppose a soft link (SL) exists between the $(i-1)^{th}$ and the $i^{th}$ links, as shown in Fig. 5, its DH parameters are parametrically modeled with respect to a vector of control parameters, denoted as $\mathbf{x}$. The transformation of the SL [19] is then given by:

$$ \mathbf{T}_{SL} = \begin{bmatrix} \cos\theta_{SL}(\mathbf{x}) & -\sin\theta_{SL}(\mathbf{x}) & 0 & 0 \\ \sin\theta_{SL}(\mathbf{x}) & \cos\theta_{SL}(\mathbf{x}) & 0 & 0 \\ 0 & 0 & 1 & d_{SL}(\mathbf{x}) \\ 0 & 0 & 0 & 1 \end{bmatrix} \cdot \begin{bmatrix} 1 & 0 & 0 & a_{SL}(\mathbf{x}) \\ 0 & \cos\alpha_{SL}(\mathbf{x}) & -\sin\alpha_{SL}(\mathbf{x}) & 0 \\ 0 & \sin\alpha_{SL}(\mathbf{x}) & \cos\alpha_{SL}(\mathbf{x}) & 0 \\ 0 & 0 & 0 & 1 \end{bmatrix} \quad (3) $$

where $q_{SL}(\mathbf{x})$, $d_{SL}(\mathbf{x})$, $a_{SL}(\mathbf{x})$ and $a_{SL}(\mathbf{x})$ are the parametrically modeled axis angle, link offset, link length and twisted angle of the SL, respectively. Therefore, the end effector of a soft robot with $N$ serially connected soft links can be determined by:

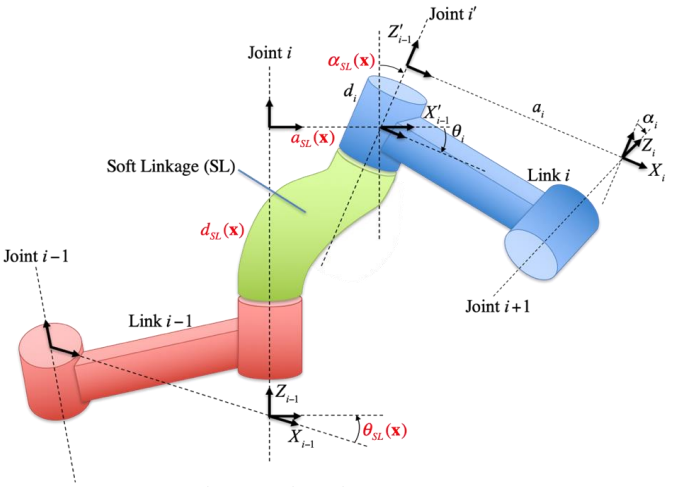


Fig. 5. Parametric DH functions for soft actuator kinematics, where each DH parameter would be parametrically functioned with the design parameter of soft finger actuation.

$$ {}^0\mathbf{P}(\mathbf{x}) = {}^0\mathbf{T}_1(\mathbf{x}) \cdot {}^1\mathbf{T}_2(\mathbf{x}) \cdots {}^{i-1}\mathbf{T}_i(\mathbf{x}) \cdots {}^{N-1}\mathbf{T}_N(\mathbf{x}) \cdot {}^N\mathbf{P} \quad (4) $$

Fig. 6 shows the experimental setup of the soft finger actuations on an optical table. The soft finger was dyed to black color for better contrast of the image-based measurements. Six red circular labels were attached to six different spots on the soft finger. Fig. 7 shows how the soft finger deforms under various levels of pulling cable forces.

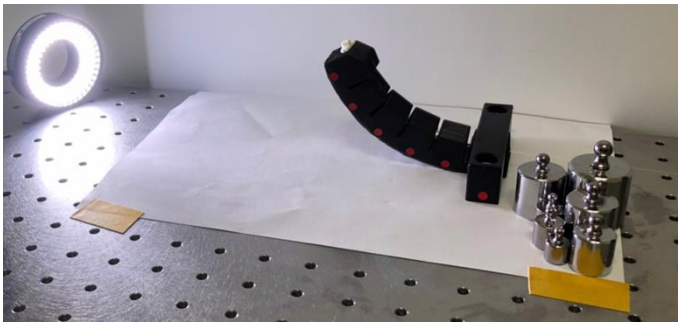

Fig. 6. Experimental setup for soft finger actuation measurements, where the soft finger was dyed to black color for better contrast in the visual inspection, multiple red circular markers were used to reveal the nonlinear deformation of the soft finger after actuation, and weights were used to pull the cable that actuates the soft finger.

Because there is no exact way to define the joint locations in a soft actuator, this paper presents 4 different kinds of SL considerations, as shown in Fig. 8. The centers of the red circular labels were chosen as the locations of axes $Z_0,..,Z_5$. Fig. 8 (a) is the consideration of 5 SLs, where $a_{ij}$ stands for the link length between the axes $Z_i$ and $Z_j$; $q_{ijk}$ stands for the angle between $\overline{Z_iZ_j}$ and $\overline{Z_jZ_k}$; $q_{0i}$ stands for the angle of the $\overline{Z_0Z_i}$. Fig. 8 (b) shows a different consideration of 3 SLs as Fig. 8 (c) and (d) show the 2-SL and 1-SL considerations, respectively. TABLES I-IV show the link lengths and axis angles under different pulling forces for the considerations of 5 SLs, 3 SLs, 2 SLs and 1 SL, respectively.

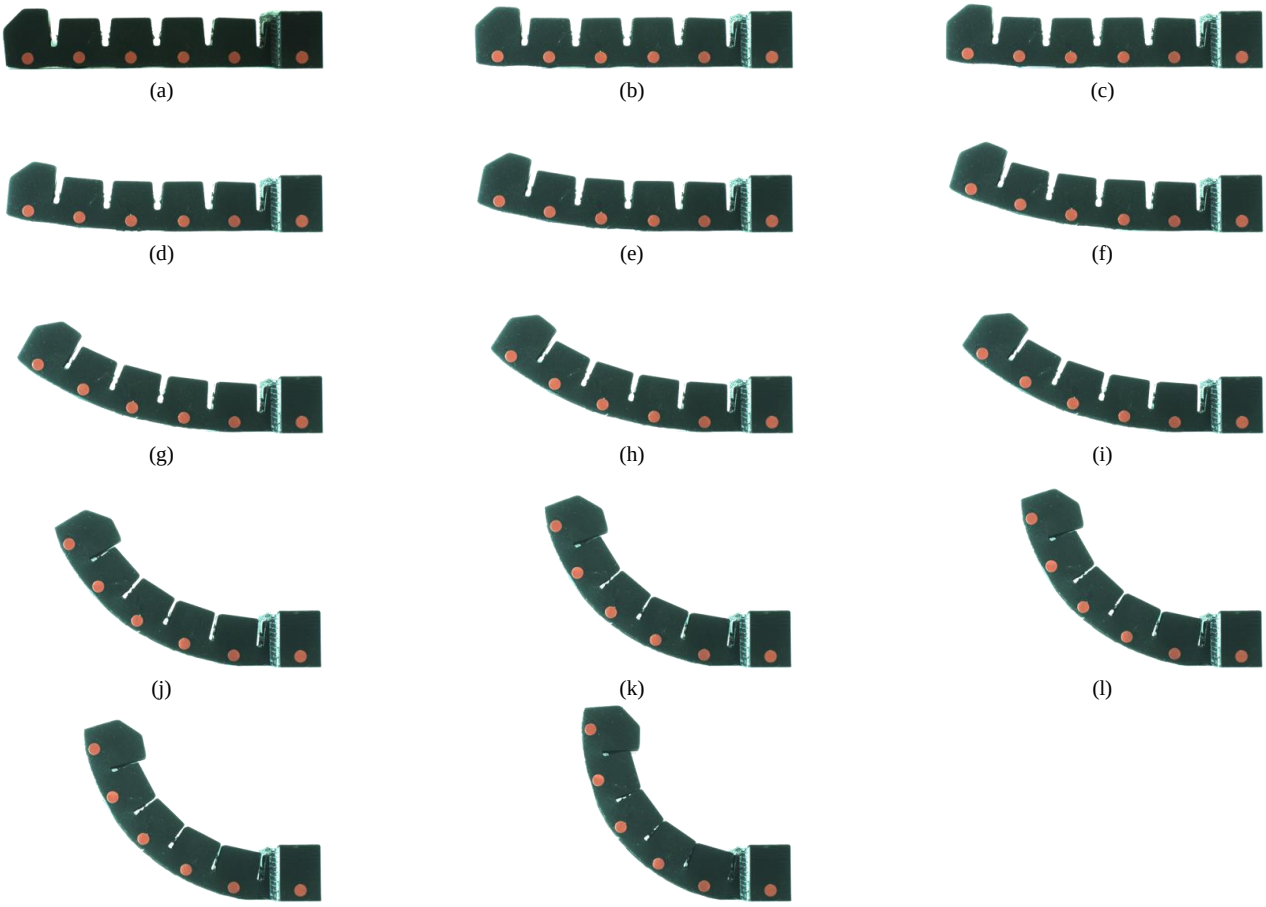

Fig. 7. Actuation of a soft finger under different pulling force: (a) original configuration; (b) 0.49 N; (c) 0.98 N; (d) 1.47 N; (e) 1.96 N; (f) 2.45 N; (g) 2.94 N; (h) 3.43 N; (i) 3.92 N.

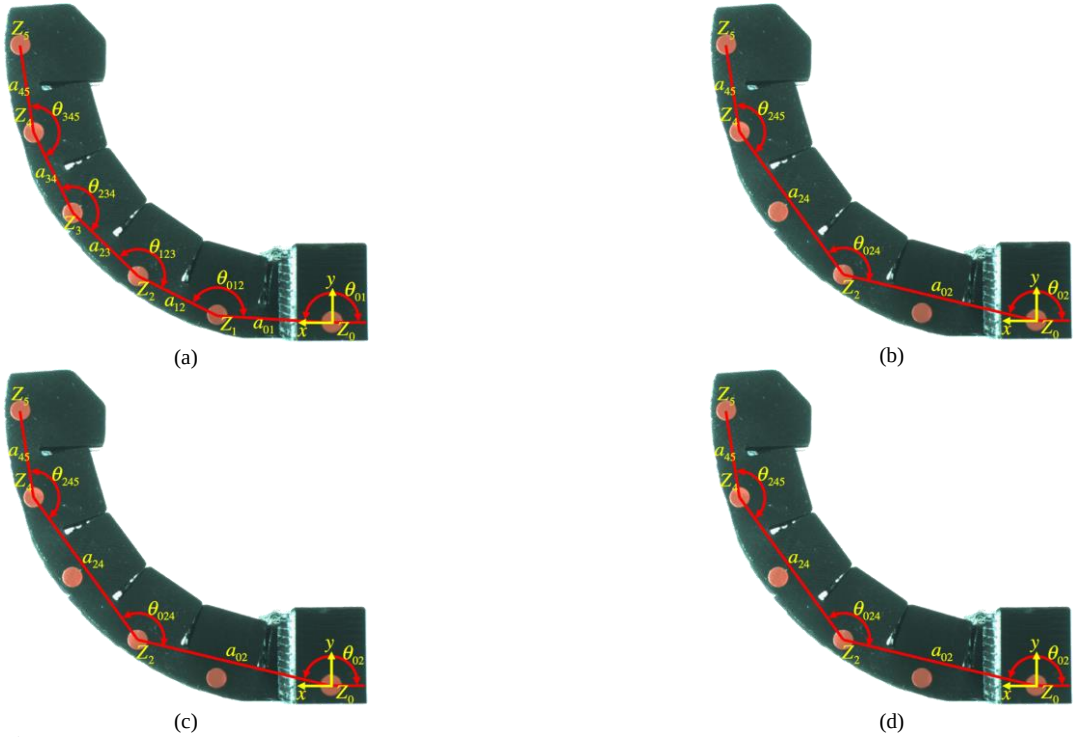


Fig. 8. Notations of link lengths and angles in the (a) 5-SL, (b) 3-SL, (c) 2-SL and (d) 1-SL considerations.

TABLE I
EXPERIMENTAL MEASUREMENTS OF LINK LENGTHS AND AXIS ANGLES FOR THE 5-SL CONSIDERATION

| Actuation force (N) | $a_{01}$ (mm) | $a_{12}$ (mm) | $a_{23}$ (mm) | $a_{34}$ (mm) | $a_{45}$ (mm) | $180-\theta_{01}$ (°) | $180-\theta_{012}$ (°) | $180-\theta_{123}$ (°) | $180-\theta_{234}$ (°) | $180-\theta_{345}$ (°) |
|---|---|---|---|---|---|---|---|---|---|---|
| 0 | 28.33 | 22.00 | 22.67 | 22.00 | 22.00 | 0.00 | 0.00 | 0.00 | 0.00 | 0.00 |
| 0.49 | 28.67 | 21.67 | 22.33 | 22.33 | 22.00 | 0.00 | 0.00 | 0.00 | 0.00 | 0.00 |
| 1.47 | 28.67 | 21.67 | 22.33 | 22.37 | 21.87 | 0.00 | 0.00 | 0.00 | 3.42 | 4.47 |
| 2.45 | 28.33 | 21.68 | 22.73 | 22.16 | 22.03 | 0.00 | 1.76 | 2.44 | 7.95 | 5.46 |
| 3.43 | 28.33 | 21.79 | 22.56 | 22.24 | 22.30 | 0.00 | 6.15 | 6.66 | 11.07 | 7.68 |
| 4.41 | 28.34 | 21.91 | 22.66 | 22.20 | 22.28 | 0.67 | 12.52 | 13.00 | 15.16 | 14.01 |
| 5.39 | 28.35 | 21.73 | 22.65 | 22.60 | 22.10 | 2.02 | 18.64 | 12.33 | 19.80 | 14.12 |
| 6.37 | 28.38 | 21.91 | 22.63 | 22.66 | 22.25 | 3.37 | 22.81 | 18.82 | 18.81 | 17.57 |

TABLE II
EXPERIMENTAL MEASUREMENTS OF LINK LENGTHS AND AXIS ANGLES FOR THE 3-SL CONSIDERATION

| Actuation force (N) | $a_{02}$ (mm) | $a_{24}$ (mm) | $a_{45}$ (mm) | $180-\theta_{02}$ (°) | $180-\theta_{024}$ (°) | $180-\theta_{245}$ (°) |
|---|---|---|---|---|---|---|
| 0 | 50.33 | 44.67 | 22.00 | 0.00 | 0.00 | 0.00 |
| 0.49 | 50.33 | 44.67 | 22.00 | 0.00 | 0.00 | 0.00 |
| 1.47 | 50.33 | 44.69 | 21.87 | 0.00 | 1.71 | 6.17 |
| 2.45 | 50.00 | 44.78 | 22.03 | 0.76 | 7.37 | 9.48 |
| 3.43 | 50.05 | 44.59 | 22.30 | 2.67 | 15.63 | 13.25 |
| 4.41 | 49.95 | 44.47 | 22.28 | 6.13 | 27.56 | 21.67 |
| 5.39 | 49.43 | 44.58 | 22.10 | 10.10 | 32.78 | 24.04 |
| 6.37 | 49.32 | 44.68 | 22.25 | 13.28 | 41.13 | 26.97 |

TABLE III
EXPERIMENTAL MEASUREMENTS OF LINK LENGTHS AND AXIS ANGLES FOR THE 2-SL CONSIDERATION

| Actuation force (N) | $a_{03}$ (mm) | $a_{35}$ (mm) | $180-\theta_{03}$ (°) | $180-\theta_{035}$ (°) |
|---|---|---|---|---|
| 0 | 73.00 | 44.00 | 0.00 | 0.00 |
| 0.49 | 72.67 | 44.33 | 0.00 | 0.00 |
| 1.47 | 72.67 | 44.21 | 0.00 | 5.62 |
| 2.45 | 72.70 | 44.15 | 1.84 | 13.04 |
| 3.43 | 72.37 | 44.43 | 5.82 | 21.90 |
| 4.41 | 71.66 | 44.15 | 12.36 | 36.01 |
| 5.39 | 70.85 | 44.36 | 17.24 | 42.53 |
| 6.37 | 69.59 | 44.38 | 23.13 | 49.39 |

TABLE IV
EXPERIMENTAL MEASUREMENTS OF LINK LENGTHS AND AXIS ANGLES FOR THE 1-SL CONSIDERATION

| Actuation force (N) | $a_{05}$ (mm) | $180-\theta_{05}$ (°) |
|---|---|---|
| 0 | 117.00 | 0.00 |
| 0.49 | 117.00 | 0.00 |
| 1.47 | 116.75 | 2.13 |
| 2.45 | 116.14 | 6.76 |
| 3.43 | 114.80 | 14.12 |
| 4.41 | 110.47 | 25.95 |
| 5.39 | 107.80 | 33.40 |
| 6.37 | 104.09 | 42.01 |

TABLE V
RESULTS OF SOFT FINGER KINEMATICS

| Actuation force (N) | True coordinate of $Z_5$ (mm) | Estimated $Z_5$ based on 5-SL consideration / Error (mm) | Estimated $Z_5$ based on 3-SL consideration / Error (mm) | Estimated $Z_5$ based on 2-SL consideration / Error (mm) | Estimated $Z_5$ based on 1-SL consideration / Error (mm) |
|---|---|---|---|---|---|
| 0.98 | [117.00, 1.33] | [116.91, 0.11] / 1.23 | [116.97, 0.1] / 1.23 | [116.98, 0.1] / 1.24 | [117.31, 0.12] / 1.25 |
| 1.96 | [116.33, 8.33] | [116.33, 8.09] / 0.24 | [116.35, 8.09] / 0.25 | [116.34, 8.1] / 0.23 | [116.42, 8.11] / 0.24 |
| 2.94 | [112.67, 24.67] | [113.33, 21.96] / 2.79 | [113.29, 21.95] / 2.79 | [113.25, 21.97] / 2.76 | [113, 21.89] / 2.80 |
| 3.92 | [105.33, 38.17] | [106.27, 38.25] / 0.94 | [106.22, 38.24] / 0.89 | [106.19, 38.23] / 0.86 | [106.01, 38.14] / 0.67 |
| 4.90 | [92.33, 56.33] | [95.39, 53.46] / 4.19 | [95.38, 53.46] / 4.19 | [95.44, 53.43] / 4.25 | [95.58, 53.54] / 4.28 |
| 5.88 | [88.33, 61.00] | [83.04, 65.27] / 6.8 | [83.06, 65.28] / 6.79 | [83.13, 65.28] / 6.74 | [83.29, 65.45] / 6.72 |

The load conditions and the corresponding measures of link lengths and axis angles in Tables 1-4 were used to build the parametric models of the DH functions. In this paper, cubic polynomial functions were used for the parametric modeling. Those DH functions were then used to estimate the end effector coordinates ( $Z_5$ ) under some other conditions of pulling forces, as shown in TABLE V. TABLE V also shows the accuracy of the parametric models based on the considerations of 5 SLs, 3 SLs, 2 SLs and 1 SL, where the error is computed by the distance between the true coordinate of $Z_5$ and the estimate coordinate. The results showed the parametric models based on various numbers of soft links had consistent estimations of the end effector coordinates. The differences between each kind of model were within 0.27 mm (i.e. the largest difference was

between 5-SL and 1-SL considerations under force of 3.92 N). Due to the large deformation of the soft finger as the actuation force was greater than 4 N, the cubic polynomial fitting was less accurate. The largest error was 6.8 mm.

## IV. Force Analysis of the Soft Finger

This paper utilized a simple force model, as shown in Fig. 9, to estimate the gripping force of the soft finger. For visual measurement of the finger deformation, the PDMS was dyed to black color. Several red circular labels were attached to the finger as the feature points in visual measurements. The x-y coordinate, indicated as point O, was defined at the center of the very left red circular label, as shown in Fig. 9. The center of the very right label was chosen as the investigated end point and its coordinate was given by [X, Y]. As the cable was pulled by a force F, the soft finger actuated and the end point coordinate moved with respect to F; therefore, X and Y are functions of F.

Yang, et al. [20] used visual measurements to obtain the coordinates of [X, Y] under various levels of F. The experimental results are shown in TABLE VI. The value of d represents the pulling distance, as shown in Fig. 9. The functions of X(F), Y(F) and d(F) were parametrically modeled as follows:

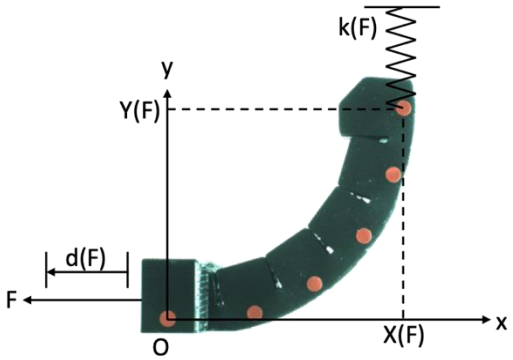


Fig. 9. A force model to estimate gripping force.

$$X(F) = a_1F^3 + a_2F^2 + 117 \quad (5)$$

$$Y(F) = a_3F^3 + a_4F^2 \quad (6)$$

$$d(F) = a_5F^3 + a_6F^2 \quad (7)$$

where $a_1$ to $a_6$ are coefficients to be determined by curve fitting. The first-ordered terms were assumed to be zero in the Eqs. (5) to (7) because the derivatives of X, Y and d with respect to F were close to zero as F = 0 N. Least Square Approximations (LSA) were used to estimate the coefficients $a_1$ to $a_6$. The fitted curves in the interval of F = [0, 6.37] were then given as:

$$X(F) = -0.0918F^3 - 0.3926F^2 + 117 \quad (8)$$

$$Y(F) = -0.3032F^3 + 3.6505F^2 \quad (9)$$

$$d(F) = -0.0892F^3 + 0.8478F^2 \quad (10)$$

The experimental data and the fitted curves in Eqs. (8) to (10) are shown in Fig. 10. More than one mathematical model was tested for the desired curve fitting. The models given in Eqs. (8) to (10) showed good results of fitting and were able to estimate the nonlinear behavior of the soft finger, as shown in Fig. 10.

TABLE VI
Experimental Results of Soft Finger Actuations under Various Levels of Pulling Forces

| F (N) | X (mm) | Y (mm) | d (mm) |
|---|---|---|---|
| 0.00 | 117.00 | 0.00 | 0.00 |
| 0.98 | 117.00 | 1.33 | 0.55 |
| 1.47 | 116.67 | 4.33 | 1.80 |
| 1.96 | 116.33 | 8.33 | 2.64 |
| 2.45 | 115.33 | 13.67 | 3.80 |
| 2.94 | 112.67 | 24.67 | 5.46 |
| 3.43 | 111.33 | 28.00 | 5.82 |
| 3.92 | 105.33 | 38.17 | 7.47 |
| 4.41 | 99.33 | 48.33 | 9.14 |
| 4.90 | 92.33 | 56.33 | 10.32 |
| 5.39 | 90.00 | 59.33 | 10.50 |
| 5.88 | 88.33 | 61.00 | 10.49 |
| 6.37 | 77.33 | 69.67 | 11.77 |

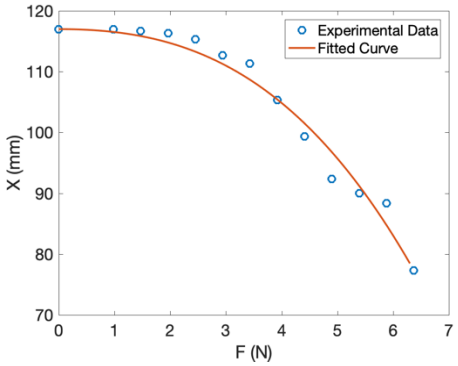


(a)

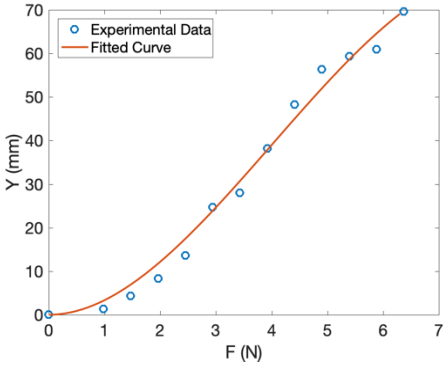


(b)

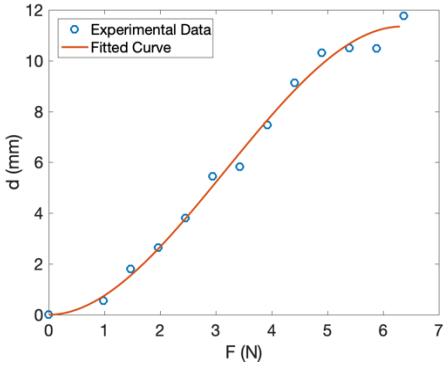


(c)

Fig. 10. Experimental data and fitted curves of (a) X(F), (b) Y(F), and (c) d(F).

To further estimate the gripping force of the soft finger, a pseudo-spring model, as shown in Fig. 9, was used to approximate the nonlinear material behavior of the soft finger under various levels of pulling force. The spring coefficient was denoted as k (unit = N/m). Assuming there was no energy loss, the work done by the pulling force was converted to the potential energy of the pseudo spring. Therefore, the following equality equation is obtained:

$$Fd = \frac{1}{2}kY^2 \tag{11}$$

Assuming the maximal deformation was reached as F = 6.37 N, the spring coefficient was then parametrically modeled as follows:

$$k(F) = b_1(F - 6.37)^2 + b_2 \tag{12}$$

where k reaches an extreme value as F = 6.37 N. LSA was again used to approximate the coefficients $b_1$ and $b_2$. At the end, the estimated nonlinear spring coefficient was given as:

$$k(F) = 0.0015(F - 6.37)^2 + 0.0308 \tag{13}$$

and it could be seen in Fig. 11. Fig. 12 shows the estimated work done and potential energy stored in the pseudo-spring, as shown in Eq. (11). Finally, the gripping force was estimated based on the product of Eqs. (9) and (13). The estimated gripping force could be seen in Fig. 13.

The utilized force model shown in Fig. 9 was a very simple one. Assuming zero energy loss and neglecting other energy conversions, the gripping force could reach up to around 2.1 N as a pulling force of 6.37 N was applied. The nonlinear behaviors of the soft finger under various levels of actuation forces were estimated with the utilized visual inspections. With the presented procedures, one could quickly estimate the gripping force of the soft finger without using any force measurement or complicated finite element analysis.

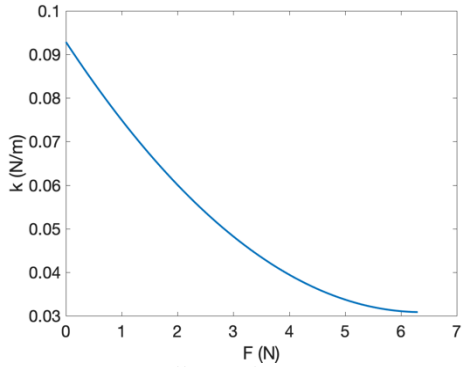

Fig. 11. Estimated spring coefficient of the nonlinear pseudo-spring.

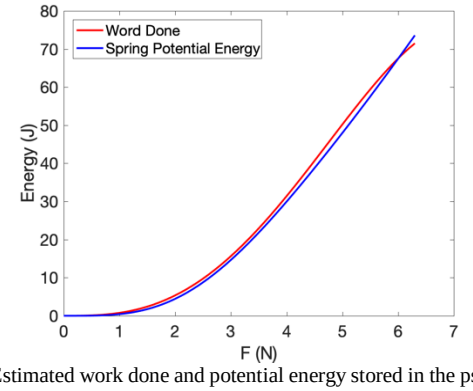

Fig. 12. Estimated work done and potential energy stored in the pseudo-spring.

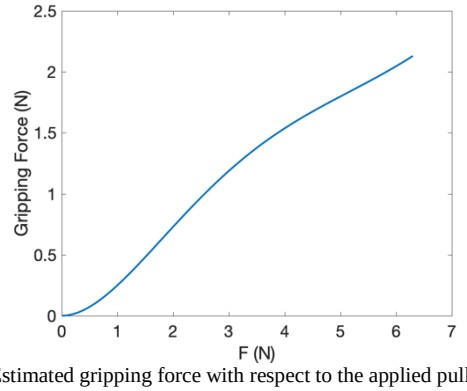

Fig. 13. Estimated gripping force with respect to the applied pulling force.

## V. Conclusions

Soft robots, which have become one of the hottest research topics in engineering and industrial applications, are however harder to model than rigid robots. The motion of soft robot is more complicated than the rigid robot because the soft robot structure deforms during actuation. Finite Element Analysis (FEA) could be used to analyze how the soft robot deforms but nonlinear FEA is required for large deformation analysis. The parametric DH functions have been developed for soft robot kinematics. This paper presented a soft finger that has a soft polydimethylsiloxane (PDMS) body and the rigid polylactic acid (PLA) bone structures. The soft finger was made by a molding process and actuated by cable pulling. The link lengths and axis angles of the soft finger were parametrically modeled for the estimations of end effector coordinates under various kinds of joint settings and load conditions. The results showed the kinematics based on different definitions of soft joints have the same results of the end effector motions. Therefore, the proposed methodologies could properly model the kinematics of various kinds of soft actuators. Furthermore, this paper presented the methodologies of visual measurement and gripping force estimation of the cable-driven soft finger. Visual inspections were used to measure and model the soft finger deformations under various levels of actuation forces. A simple force model was defined to estimate the gripping force at the tip of the soft finger. Without using any force measurement or complicated finite element analysis, the presented soft finger had a gripping force of around 2.1 N as a pulling force of 6.37 N was applied.

## VI. REFERENCES

[1] M. Cianchetti, T. Ranzani, G. Gerboni, T. Nanayakkara, K. Althoefer, P. Dasgupta, and A. Menciassi, "Soft robotics technologies to address shortcomings in today's minimally invasive surgery: the STIFF-FLOP approach," *Soft robotics*, vol. 1, no. 2, pp. 122-131, 2014, DOI. 10.1089/soro.2014.0001.

[2] C. Walsh, "Human-in-the-loop development of soft wearable robots," *Nature Reviews Materials*, vol. 3, no. 6, p. 78, 2018, DOI. 10.1038/s41578-018-0011-1.

[3] P. Polygerinos, Z. Wang, K. C. Galloway, R. J. Wood, and C. J. Walsh, "Soft robotic glove for combined assistance and at-home rehabilitation," *Robotics and Autonomous Systems*, vol. 73, pp. 135-143, 2015, DOI. 10.1016/j.robot.2014.08.014.

[4] J. Shintake, S. Rosset, B. Schubert, D. Floreano, and H. Shea, "Versatile soft grippers with intrinsic electroadhesion based on multifunctional polymer actuators," *Advanced materials*, vol. 28, no. 2, pp. 231-238, 2016, DOI. 10.1002/adma.201504264.

[5] S. Shian, K. Bertoldi, and D. R. Clarke, "Dielectric elastomer based "grippers" for soft robotics," *Advanced Materials*, vol. 27, no. 43, pp. 6814-6819, 2015, DOI. 10.1002/adma.201503078.

[6] M. Wehner, R. L. Truby, D. J. Fitzgerald, B. Mosadegh, G. M. Whitesides, J. A. Lewis, and R. J. Wood, "An integrated design and fabrication strategy for entirely soft, autonomous robots," *Nature*, vol. 536, no. 7617, pp. 451-455, 2016, DOI. 10.1038/nature19100.

[7] C. Lee, M. Kim, Y. J. Kim, N. Hong, S. Ryu, H. J. Kim, and S. Kim, "Soft robot review," *International Journal of Control, Automation and Systems*, vol. 15, no. 1, pp. 3-15, 2017, DOI. 10.1007/s12555-016-0462-3.

[8] C. D. Onal, X. Chen, G. M. Whitesides, and D. Rus, "Soft mobile robots with on-board chemical pressure generation," *Robotics Research*, pp. 525-540, Springer, 2017.

[9] P. Polygerinos, N. Correll, S. A. Morin, B. Mosadegh, C. D. Onal, K. Petersen, M. Cianchetti, M. T. Tolley, and R. F. Shepherd, "Soft robotics: Review of fluid-driven intrinsically soft devices; manufacturing, sensing, control, and applications in human-robot interaction," *Advanced Engineering Materials*, vol. 19, no. 12, p. 1700016, 2017, DOI. 10.1002/adem.201700016.

[10] J. F. Morrow, "Direct 3D Printing of Silicone Elastomer Soft Robots without Support," Thesis, Department of Mechanical, Industrial, and Manufacturing Engineering, Oregon State University, 2017.

[11] J. Paik, "Soft robot design methodology for 'push-button' manufacturing," *Nature Reviews Materials*, vol. 3, no. 6, p. 81, 2018, DOI. 10.1038/s41578-018-0014-y.

[12] G. Gerboni, A. Diodato, G. Ciuti, M. Cianchetti, and A. Menciassi, "Feedback control of soft robot actuators via commercial flex bend sensors," *IEEE/ASME Transactions on Mechatronics*, vol. 22, no. 4, pp. 1881-1888, 2017, DOI. 10.1109/TMECH.2017.2699677.

[13] H. Zhang, R. Cao, S. Zilberstein, F. Wu, and X. Chen, "Toward effective soft robot control via reinforcement learning," presented at the International Conference on Intelligent Robotics and Applications, 2017, DOI. 10.1007/978-3-319-65289-4_17.

[14] H. Wang, B. Yang, Y. Liu, W. Chen, X. Liang, and R. Pfeifer, "Visual servoing of soft robot manipulator in constrained environments with an adaptive controller," *IEEE/ASME Transactions on Mechatronics*, vol. 22, no. 1, pp. 41-50, 2017, DOI. 10.1109/TMECH.2016.2613410.

[15] Y. Ansari, M. Manti, E. Falotico, M. Cianchetti, and C. Laschi, "Multiobjective optimization for stiffness and position control in a soft robot arm module," *IEEE Robotics and Automation Letters*, vol. 3, no. 1, pp. 108-115, 2018, DOI. 10.1109/LRA.2017.2734247.

[16] H.-C. Lu, C.-H. Kuo, and P. T. Lin, "A Neural Network Simulation for Tip Displacement of the Large-Deflection Beams with an Obstacle Based on ANSYS," presented at the 2018 International Conference on Advanced Robotics and Intelligent Systems (ARIS 2018), Taipei, Taiwan, 2018.

[17] E. Shahabi, Y.-T. Yao, C.-H. Chuang, P. T. Lin, and C.-H. Kuo, "Design and Testing of 2-Degree-of-Freedom (DOF) Printable Pneumatic Soft Finger," presented at the The 6th IFToMM International Symposium on Robotics and Mechatronics (ISRM 2019), Taipei, Taiwan, 047, 2019, DOI. 10.1007/978-3-030-30036-4_27.

[18] J. Denavit and R. S. Hartenberg, "A kinematic notation for low pair mechanisms based on matrices," *Journal of Applied Mechanics*, vol. 22, pp. 215-221, 1955.

[19] P. T. Lin, E. Shahabi, K.-A. Yang, Y.-T. Yao, and C.-H. Kuo, "Parametrically Modeled DH Table for Soft Robot Kinematics: Case Study for A Soft Gripper," presented at the The 15th IFToMM World Congress, Krakow, Poland, 453, 2019, DOI. 10.1007/978-3-030-20131-9_62.

[20] K.-A. Yang, Y.-T. Yao, W.-Y. Tan, and P. T. Lin, "Investigation of Soft Actuator Kinematics Based on Parametric DH Functions," presented at the International Conference on Advanced Technology Innovation 2019 (ICATI2019), Sapporo, Hokkaido, Japan, SCG9003, 2019.

**Po Ting Lin** received the M.S. and Ph.D. degrees in the Department of Mechanical and Aerospace Engineering from Rutgers University, New Brunswick, New Jersey, USA in 2007 and 2010, respectively. He is currently an Associate Professor in the Department of Mechanical Engineering, National Taiwan University of Science and Technology, Taipei, Taiwan. His current research interests and publications are in the areas of Machine Vision, Robotics, Machine Learning, Reliability-Based Design Optimization, and Multidisciplinary Design Optimization

**Kai-An Yang** received the M.S. degree in the Department of Mechanical Engineering, National Taiwan University of Science and Technology, Taipei, Taiwan in July 2019.

**Cheng-Hsiu Chuang** received the M.S. degree in the Department of Mechanical Engineering, National Taiwan University of Science and Technology, Taipei, Taiwan in July 2020.

**Yu-Ta Yao** received the M.S. degree in the Department of Mechanical Engineering, National Taiwan University of Science and Technology, Taipei, Taiwan in July 2020.